


## Article

# Experimental Study on Two PCM Macro-Encapsulation Designs in a Thermal Energy Storage Tank

David Vérez , Emiliano Borri , Alicia Crespo, Boniface Dominick Mselle , Álvaro de Gracia ,  
Gabriel Zsembinszki  and Luisa F. Cabeza 

GREiA Research Group, Universitat de Lleida, Pere de Cabrera s/n, 25001 Lleida, Spain;  
david.verez@udl.cat (D.V.); emiliano.borri@udl.cat (E.B.); alicia.crespo@udl.cat (A.C.);  
boniface.mselle@udl.cat (B.D.M.); adegracia@diei.udl.cat (Á.d.G.); gabriel.zsembinszki@udl.cat (G.Z.)

\* Correspondence: luisaf.cabeza@udl.cat; Tel.: +34-973-003-576

**Abstract:** The use of latent heat thermal energy storage is an effective way to increase the efficiency of energy systems due to its high energy density compared with sensible heat storage systems. The design of the storage material encapsulation is one of the key parameters that critically affect the heat transfer in charging/discharging of the storage system. To fill the gap found in the literature, this paper experimentally investigates the effect of the macro-encapsulation design on the performance of a lab-scale thermal energy storage tank. Two rectangular slabs with the same length and width but different thickness (35 mm and 17 mm) filled with commercial phase change material were used. The results show that using thinner slabs achieved a higher power, leading to a reduction in the charging and discharging time of 14% and 30%, respectively, compared with the thicker slabs. Moreover, the variation of the heat transfer fluid flow rate has a deeper impact on the temperature distribution and the energy charged/released when thicker slabs were used. The macro-encapsulation design did not have a significant impact on the discharging efficiency of the tank, which was around 85% for the operating thresholds considered in this study.

**Keywords:** thermal energy storage; latent heat thermal energy storage; phase change materials (PCM); macro-encapsulation; rectangular slab; experimental study



**Citation:** Vérez, D.; Borri, E.; Crespo, A.; Mselle, B.D.; de Gracia, Á.; Zsembinszki, G.; Cabeza, L.F.

Experimental Study on Two PCM Macro-Encapsulation Designs in a Thermal Energy Storage Tank. *Appl. Sci.* **2021**, *11*, 6171. <https://doi.org/10.3390/app11136171>

Academic Editor: Ioannis Kartsonakis

Received: 25 May 2021

Accepted: 30 June 2021

Published: 2 July 2021

**Publisher's Note:** MDPI stays neutral with regard to jurisdictional claims in published maps and institutional affiliations.



**Copyright:** © 2021 by the authors. Licensee MDPI, Basel, Switzerland. This article is an open access article distributed under the terms and conditions of the Creative Commons Attribution (CC BY) license (<https://creativecommons.org/licenses/by/4.0/>).

## 1. Introduction

The use of thermal energy storage (TES) has been proved as an effective way to enhance the penetration of renewable energy into energy systems. Amongst all thermal storage technologies, latent heat thermal energy storage (LHTES) received the attention of several researchers over the last decade due to its high energy density and the wide range of applications [1]. Buildings, for example, represent one of the most common applications of the integration of LHTES as an active or passive system [2–4]. For the active systems, TES can be used in HVAC components or systems to balance the supply of domestic hot water and heating/cooling demand when renewables are used [5,6], or to reduce the energy consumption through peak load shifting [7], or free cooling techniques [8]. On the other hand, passive systems are directly integrated into the building envelope to reduce the energy demand [9,10]. Other common applications where LHTES can be integrated include solar thermal power plants, such as concentrated solar power (CSP) [11], solar cooling applications [12], district heating or cooling [13], waste heat recovery [14], solar process heat [15], or cryogenic applications [16].

The principle behind LHTES is the use of phase change materials (PCM) as the storage medium, allowing to store thermal energy at a nearly constant temperature exploiting the latent heat during the phase transition, for which the most common one is from solid to liquid to minimize the impact of volume expansions [17]. One of the weaknesses of PCM is its low thermal conductivity that negatively affects the thermal power involved in the charging and discharging processes of the energy storage system. Indeed, this represents

one of the main challenges facing the implementation of PCM in various applications. However, different strategies and techniques that can be used to improve thermal conductivity were investigated in the literature. The main solutions that were extensively studied are the increase in the convection coefficient of heat transfer by means of dynamic systems, the addition of particles (such as carbon elements, metallic particles, and nanoparticles), the inclusion of PCM in a metallic matrix, and the increase in the heat transfer area by using fins, and micro and macro-encapsulation [18–20].

On one hand, PCM micro-encapsulation allows increasing heat transfer surface between the PCM and the heat transfer fluid. However, for PCM microencapsulation, complex and expensive processes are needed, such as spray drying (physical method) or interfacial polymerization (chemical methods) [21]. On the other hand, macro-encapsulation requires a simpler making process resulting in a lower cost [22]. Furthermore, larger sizes of the container also allow an increase in the mechanical stability of systems [23]. Macro-encapsulated PCM can be designed with different geometries mainly based on rectangular [24], cylindrical [25,26], and spherical shapes [27] that can be adapted to different applications. The effect of the design of macro-encapsulation on the heat transfer performance is mostly analyzed by numerical analysis with only a few experimental studies available in the literature, highlighting a research gap. Amongst the experimental studies available, Erlbeck et al. [28] and Al-Yasiri and Szabó [29] experimentally investigated the thermal behavior of concrete blocks with different shapes of microencapsulated PCM. Ismail and Moraes [30] numerically and experimentally evaluated spherical containers made with different geometries and materials and filled with PCM for cold storage domestic applications. This paper experimentally analyzes the effect of two different geometries of macro-encapsulated PCM in rectangular slabs on the performance of an energy storage tank. The analyzed TES tank is part of the generic heating system designed for the EU funded project SWS-HEATING (GA 764025). In particular, the PCM tank is used in the system as a thermal buffer to store the solar energy at low-grade temperature ( $15 \pm 5^\circ\text{C}$ ) to be supplied to a novel seasonal TES based on selective water sorbent materials. To the best of the authors knowledge, very few experimental studies on PCM tanks with rectangular slabs were published in the literature. One of the first papers was published by Moreno et al. [31] in which the performance of a TES tank filled with commercial PCM encapsulated in rectangular slabs was compared with the same tank filled with water. The results showed that the energy storage capacity of the tank filled with PCM was increased by 35.5% compared with the same tank filled with water. Another study published by D'Avignon and Kummert [32] reported the results of experimental tests performed to study the behavior of a real-scale PCM storage at different operating conditions. One of the main conclusions from the study was that the PCM hysteresis and sub-cooling effects deviate the expected behavior from the experimental results. Liu et al. [33] used the experimental results obtained from the testing of a PCM tank filled with rectangular slabs containing a PCM with a sub-zero melting temperature ( $-26.7^\circ\text{C}$ ) suitable for refrigerated transport, and glycol as heat transfer fluid. The developed model was based on a one-dimensional approach considering the temperature variations along direction of the heat transfer fluid showing a good agreement with the test. All experimental studies mentioned were carried out using a fixed design of the PCM tank without changing any boundaries related to the geometry or the configuration of the storage tank.

However, the geometrical design of the PCM encapsulation has a large influence on the thermal behavior of the PCM affecting the melting and the solidification process, and consequently the heat transfer [34]. In the case of rectangular shapes, the aspect ratio (height to width ratio) is a parameter that has to be taken into account in the design of TES tanks [21]. This paper shows for the first time a comparison based on experimental results of the thermal behavior of two different designs of macro-encapsulation of rectangular PCM slabs. The behavior of a thermal energy storage tank was analyzed using commercial PCM slabs with different thicknesses. The comparison of the two designs was done in terms of temperature profile, heat transfer rate, and energy obtained during the discharging process.

The main results obtained from the experimental tests reported in this paper can be used as a reference for institutions and manufacturers to optimize future designs of PCM tanks.

## 2. Materials and Methods

### 2.1. Materials

The PCM selected in this experimentation was PlusICE S15 (hydrated salt), supplied by PCM products, United Kingdom [35]. The main thermophysical properties of this material are shown in Table 1. Moreover, water was used as the heat transfer fluid (HTF).

**Table 1.** Thermophysical properties of PlusICE S15 [35].

Properties	Value
Melting temperature [°C]	15
Latent heat [J/g]	180
Specific heat capacity [kJ/kg·K]	1.90
Density [kg/m <sup>3</sup> ]	1700–1800
Thermal conductivity [W/(m·K)]	0.43
Maximum operation temperature [°C]	60

### 2.2. Experimental Set-Up

The experiments presented in this paper were carried out at the laboratory of the GREiA research group at the University of Lleida in Spain, in a set-up designed to test and characterize latent heat TES systems for mid-low temperature applications ( $-20\text{ °C} < T < 100\text{ °C}$ ). Figure 1 shows a detailed schematic diagram of the experimental set-up composed by a 25 L inertia water tank, whose temperature is controlled by a vapor compression cooling unit (Zanotti model GCU2030ED01B [36]) of 5 kW cooling power, two immersion thermostats (OVAN TH100E-2kW [37], and JP SELECTA-1kW [38]). The set-up also integrates: two variable speed pumps, used to control the flow and inlet temperature at the TES system; and a flow meter Badger meter type ModMAG M1000 [39] with an accuracy of  $\pm 0.25\%$  of the actual value, and the latent heat TES storage. The connections between components were joined using 0.5" diameter copper pipes insulated with  $18 \times 0.9$  mm polyurethane tubes. The data acquisition system used consisted of 3 STEP DL-01 data logger [40] connected to a computer that integrates a system control and data acquisition software (SCADA) developed in InduSoft Web Studio [41]. The data recording interval was set to 10 s.

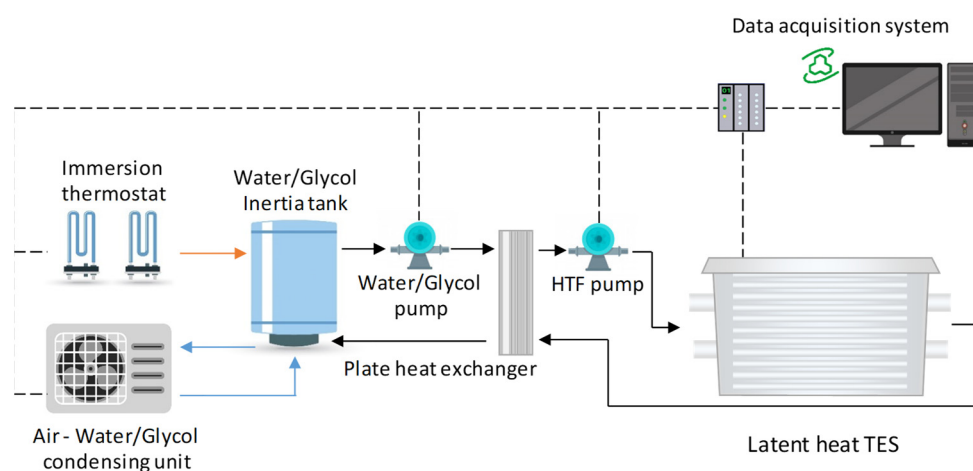


**Figure 1.** Schematic view of the experimental set-up used to perform the experimentation.

Figure 2 shows the PCM storage tank connected to the experimental set-up. The tests were carried out with two different PCM macro-encapsulation designs, namely, ThinICE and FlatICE (Figure 3). The containers were made in HDPE. The external dimensions of

each design are reported in Figure 3, characterized by presenting similar length and width (A and B), but different thickness, with FlatICE dimensions being double that of ThinICE (C). Furthermore, the (D) dimension reveals that the use of thin macro-encapsulation enabled a larger distance between the slabs, increasing the space that allows circulating the HTF through the TES tank. Considering the aforementioned dimensions shown in Figure 3, the use of ThinICE encapsulation allowed fitting a larger number of slabs inside the tank, but less amount of latent storage material compared with the FlatICE, as shown in Table 2.



Figure 2. Latent heat TES.

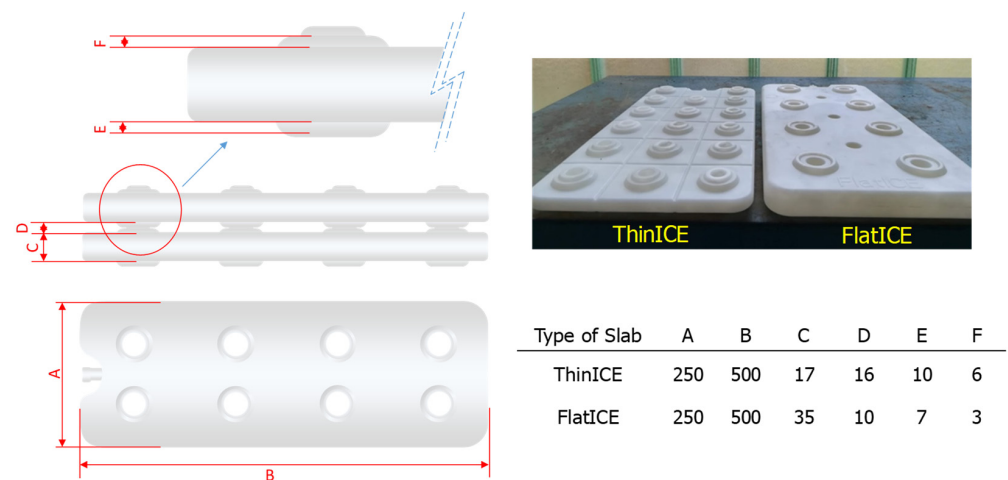
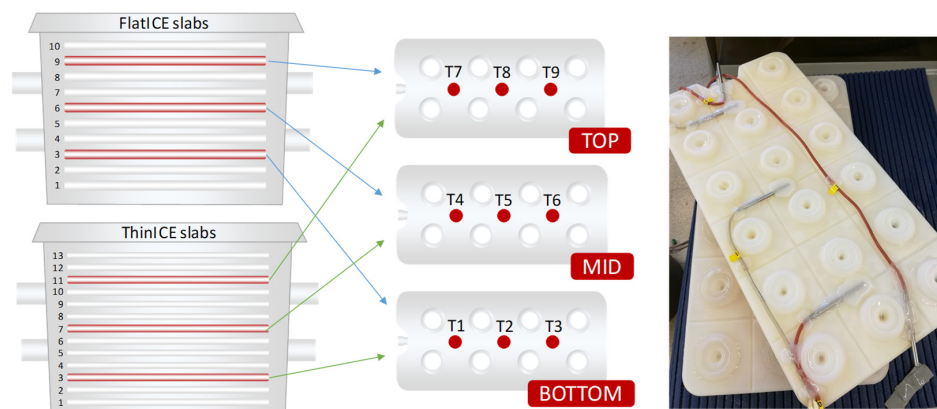


Figure 3. ThinICE and FlatICE slabs encapsulation. Dimensions in millimeters.

Table 2. Total weight of PCM inside the tank.

Properties	FlatICE	ThinICE
Capacity of the slab [liters]	3.2	1.7
Weight of the container [kg]	0.55	0.5
Total weight of a single slab [kg]	6.7	3.8
Number of slabs inside the PCM tank	10	13
Total amount of PCM inside the tank [kg]	61.5	41.9
Total weight of the slabs inside the tank [kg]	67	49.4

The temperature inside the PCM storage was measured using nine Pt-100 class B, IEC 60751 standard type, with an accuracy of  $(0.3 + 0.005 \cdot T)$ . The sensors were fixed as shown in Figure 4 to the external surface of three different PCM slabs placed at the bottom, middle, and top of the tank, respectively. Moreover, two additional Pt-100 class A IEC 60751 standard type with an accuracy of  $(0.15 + 0.002 \cdot T)$  sensors were placed at the inlets and outlets of the storage tank.



**Figure 4.** Temperature sensors location inside the storage tank.

### 2.3. Methodology

The experimental tests consisted of performing four different charging and discharging processes to evaluate the effect of the PCM macro-encapsulation design and the flow rate on the temperature distribution, heat transfer rate, and energy stored/released. At least three repetitions of each process were performed to ensure repeatability. A summary of the flow rates and temperatures used in the experimentation is shown in Table 3. Furthermore, the heat losses in the worst-case scenario analyzed represent 4% of the charging/discharging energy, therefore the analysis of heat losses was not included in the paper.

**Table 3.** Summary of the main parameters of the processes.

Process	Slab Type	Flow Rate [L/min]	HTF Inlet Temperature [°C]	PCM Tank Average Initial Temperature [°C]	Code
Charge	ThinICE	2	25	$5 \pm 1$	C_ThinICE_2L
Charge	ThinICE	4	25	$5 \pm 1$	C_ThinICE_4L
Charge	FlatICE	2	25	$5 \pm 1$	C_FlatICE_2L
Charge	FlatICE	4	25	$5 \pm 1$	C_FlatICE_4L
Discharge	ThinICE	2	5	$25 \pm 1$	D_ThinICE_2L
Discharge	ThinICE	4	5	$25 \pm 1$	D_ThinICE_4L
Discharge	FlatICE	2	5	$25 \pm 1$	D_FlatICE_2L
Discharge	FlatICE	4	5	$25 \pm 1$	D_FlatICE_4L

To perform a charging process, HTF was first circulated through the PCM tank until all sensors inside the tank reached a temperature of  $5 \pm 1$  °C. Then, the HTF inlet temperature was set at  $25 \pm 1$  °C and the flow rate was set to the corresponding value of the experiment shown in Table 3. The charging process was considered complete when the HTF temperature at the outlet of the tank reached 25 °C. To perform a discharging process, HTF was first circulated through the PCM tank until all sensors inside the tank reached a temperature of  $25 \pm 1$  °C. Then, the HTF inlet temperature was set at  $5 \pm 1$  °C and the flow rate was set to the corresponding value of the experiment in Table 3. The discharging process was considered complete when the HTF at the outlet of the tank reached 7 °C. This value was used instead of 5 °C because a minimum temperature difference of 2 °C was assumed between inlet and outlet of the storage tank as a constraint from the demand side.



## 2.4. Uncertainties Analysis

The impact of the uncertainties in the calculated parameters from the different measurements was evaluated by performing an uncertainty analysis using the Kline McClintock method. The uncertainties of the different monitored parameters are shown in Table 4. HTF specific heat capacity and density were calculated following the correlations presented in Equations (1) and (2) [42]:

$$\rho_{HTF} = 1.38 \cdot 10^{-5} \cdot T_{HTF}^3 - 5.63 \cdot 10^{-3} \cdot T_{HTF}^2 + 3.6 \cdot 10^{-3} \cdot T_{HTF}^1 + 1000 \quad (1)$$

$$C_{pHTF} = 2.69 \cdot 10^{-9} \cdot T_{HTF}^4 - 6.63 \cdot 10^{-7} \cdot T_{HTF}^3 + 6.67 \cdot 10^{-5} \cdot T_{HTF}^2 - 2.67 \cdot 10^{-3} \cdot T_{HTF}^1 + 4.21 \quad (2)$$

**Table 4.** Uncertainties of the different parameters involved in the analyses of the present study.

Parameter	Units	Sensor	Accuracy
Temperature	°C	Pt-100 1/5 DIN class B IEC 60751	$\pm 0.3 + 0.005 \cdot T$
Temperature	°C	Pt-100 1/5 DIN class A IEC 60751	$\pm 0.15 + 0.002 \cdot T$
Flow rate	L/min	Badger meter type ModMAG M1000	$\pm 0.25\%$

By applying Equation (3) to the different parameters [43], the uncertainties of the HTF thermophysical properties (density and specific heat) as well as of the heat transfer rates and total stored/released energy were estimated. The uncertainty of the HTF thermophysical properties and heat transfer rates was estimated at each registered time step, and then the mean value was used. Table 5 shows the average uncertainties of the HTF density, specific heat, heat transfer rate, and stored/released energy during the different processes carried out:

$$W_R = \left[ \left( \frac{\partial R}{\partial x_1} \cdot w_{x_1} \right)^2 + \left( \frac{\partial R}{\partial x_2} \cdot w_{x_2} \right)^2 + \dots + \left( \frac{\partial R}{\partial x_n} \cdot w_{x_n} \right)^2 \right]^{1/2} \quad (3)$$

where  $W_R$  is the estimated uncertainty in the final result,  $R$  the function which depends on the measured parameters,  $x_n$  is the different independent monitored parameters, and  $w_x$  is the uncertainties associated to those independent parameters.

**Table 5.** Estimated uncertainties of the HTF thermophysical properties, heat transfer rate, and cumulated energy.

Test	Density [ $\pm \text{kg/m}^3$ ]	Specific Heat [ $\pm \text{kJ/kg} \cdot ^\circ\text{C}$ ]	Heat Transfer Rate [ $\pm \text{kW}$ ]	Accumulated Energy [ $\pm \text{kJ}$ ]
C_ThinICE_2L	$\pm 1.28$	$\pm 2.44 \cdot 10^{-2}$	$\pm 0.039$	$\pm 19$
C_ThinICE_4L	$\pm 1.28$	$\pm 2.42 \cdot 10^{-2}$	$\pm 0.055$	$\pm 19$
C_FlatICE_2L	$\pm 1.27$	$\pm 2.43 \cdot 10^{-2}$	$\pm 0.038$	$\pm 23$
C_FlatICE_4L	$\pm 1.28$	$\pm 2.45 \cdot 10^{-2}$	$\pm 0.054$	$\pm 24$
D_ThinICE_2L	$\pm 5.5 \cdot 10^{-2}$	$\pm 2.95 \cdot 10^{-3}$	$\pm 0.039$	$\pm 19$
D_ThinICE_4L	$\pm 5.6 \cdot 10^{-2}$	$\pm 3.05 \cdot 10^{-3}$	$\pm 0.055$	$\pm 20$
D_FlatICE_2L	$\pm 5.3 \cdot 10^{-2}$	$\pm 2.77 \cdot 10^{-3}$	$\pm 0.039$	$\pm 23$
D_FlatICE_4L	$\pm 5.6 \cdot 10^{-2}$	$\pm 3.21 \cdot 10^{-3}$	$\pm 0.055$	$\pm 23$

## 3. Results and Discussion

### 3.1. Temperature Evolution during the Charging Process

Figure 5 shows the charging temperature profile of all sensors placed at the surface of the slabs for the two PCM encapsulation design at different flow rates. To analyze the effect of the encapsulation design in the charging duration, both slabs types were compared at

the same flow rate. Due to the higher heat transfer surface and the reduced amount of PCM (30% less according to Table 3) when using ThinICE slabs, at both flow rates, the experiment with the ThinICE slabs reached full charge ( $T_{out} = 25\text{ }^{\circ}\text{C}$ ) 14% faster than with FlatICE. Furthermore, when analyzing the impact of the flow rate, in both slab designs the experiments show that at 4 L/min the full charge is reached 60% faster than at 2 L/min.

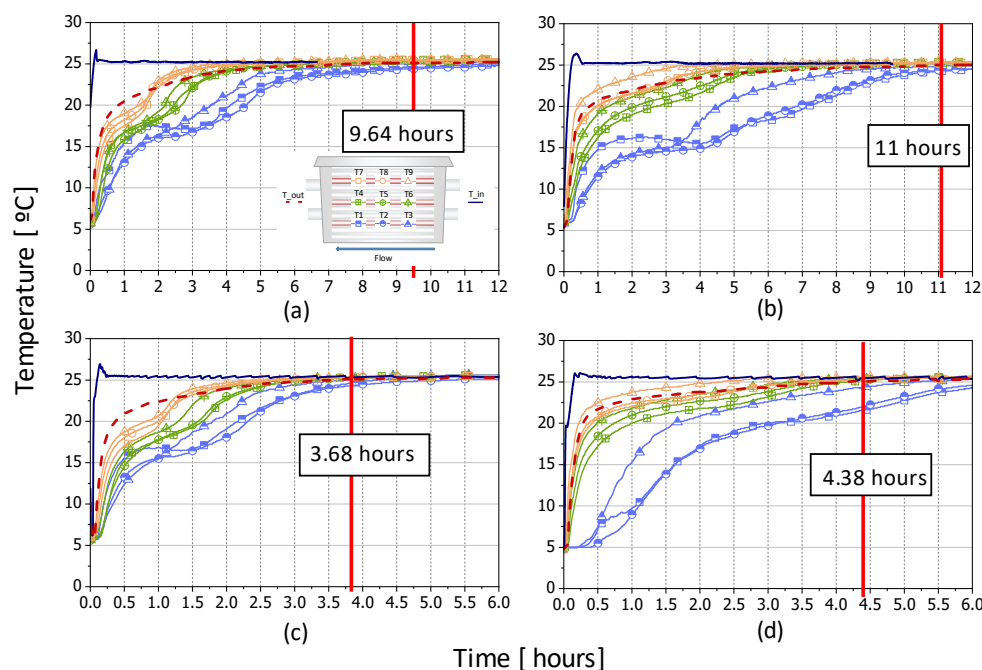


**Figure 5.** Charge PCM slab temperature profile for different slabs and HTF flow rates: (a) C\_ThinICE and 2 L/min, (b) C\_FlatICE and 2 L/min, (c) C\_ThinICE and 4 L/min, and (d) C\_FlatICE and 4 L/min. Note: The red line denotes the end of the charging experiment ( $T_{out} = 25\text{ }^{\circ}\text{C}$ ). The time axis is not presented on the same scale in all the figures.

When comparing temperature distribution inside the tank (Figure 5), a constant stratification profile between the top, middle, and bottom slabs was observed in all the experiments. This effect was more pronounced in the tests performed with FlatICE slabs in which the lower part of the tank takes longer to charge, obtaining a temperature gradient up to 15 K between the coldest and hottest regions of the tank. This can be explained by the fact that the tank with FlatICE fits a lower number of slabs, as well as presenting smaller HTF channels compared with the tank with the ThinICE design (Figure 3, Table 2). Therefore, in this tank, the opposition to the HTF flow is higher, enhancing the distribution of the latter towards the regions of the tank where the density is more similar to the HTF inlet one (i.e., upper and middle region of the tank).

### 3.2. Heat Transfer Rate Evolution and Total Energy Stored in the Charging Process

Figure 6 presents the evolution of the heat transfer rate (HTR) during the charging process of the four studied cases. Due to the characteristics of the experimental set-up, at the beginning of the experiment, the inlet temperature of the tank oscillated  $\pm 2\text{ }^{\circ}\text{C}$  with respect to the desired temperature, affecting the initial peak of the heat transfer rate. However, the inlet temperature stabilized (with  $T_{in}$  standard deviation lower than 0.3) before the temperature inside the tank reaches the latent range of the PCM. The HTR profiles showed an exponential behavior with significantly higher values during the first 20 min of the process when the heat is mainly transferred to the HTF inside the tank and, therefore, rapidly increases its temperature. Afterwards, while the PCM temperature increases, the values of the heat transfer exponentially decrease until minimum values.

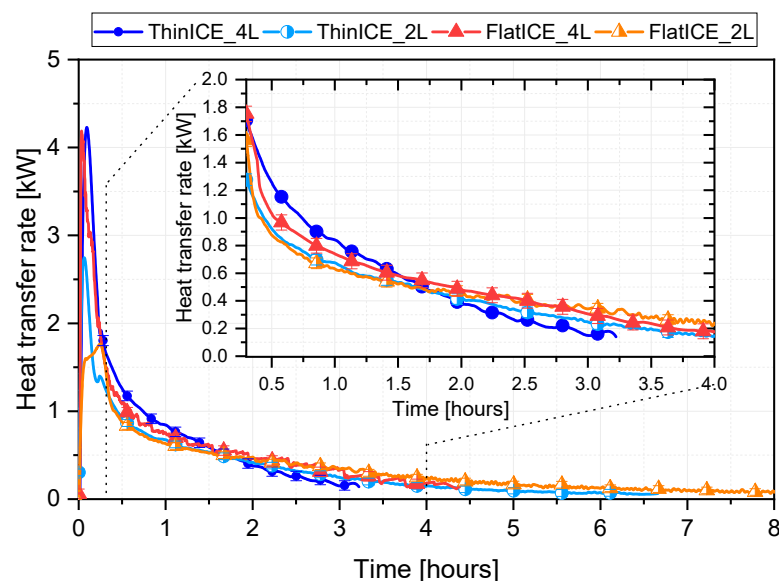


**Figure 6.** Evolution of the HTF heat transfer rate during the charging processes of the four study cases presented in this study.

During the first 1.5 h of operation, ThinICE\_2L and FlatICE\_2L showed similar HTR values, which indicates that, due to the low flow rate, the heat transfer by convection is low. Therefore, the higher heat transfer surface area existing with ThinICE slabs is not fully exploited. Moreover, after 1.5 h the HTR delivered to the ThinICE\_2L decreases faster than the one delivered to the FlatICE\_2L due to the higher amount of PCM introduced into the tank with FlatICE slabs. At a higher flow rate, heat transfer by convection increases. Therefore, during the first 1.5 h of operation, the bigger heat transfer surface area present with ThinICE\_4L slabs increases its HTR over FlatICE\_4L. After this period, and similar to the results at 2 L/min, the power delivered to the ThinICE\_4L decreased faster than the one delivered to the FlatICE\_4L.

When analyzing the effect of the flows in each slab type, the influence is greater in the tank with ThinICE slabs obtaining, after the initial peak, up to 0.4 kW more in ThinICE\_4L than in ThinICE\_2L. In the case of the tank with FlatICE, this increase drops to 0.1 kW when comparing FlatICE\_4L vs FlatICE\_2L. The latter results corroborate the statement above; the increase in heat transfer by convection, as the flow rate increases, is more pronounced in the tank with ThinICE slabs due to the larger heat transfer surface and the lower thickness of the PCM layer using this type of slab.

Figure 7 reports the total energy stored for each experiment condition. The results with ThinICE slabs show that the flow variation did not affect the total stored energy, suggesting the correct utilization of the energy storage capacity of the PCM. Conversely, when analyzing the tank with FlatICE slabs, the charging experiments at 4 L/min stored 10% less energy than the same experiment at 2 L/min. This is due to changes in the flow rate distribution between the slab channels inside the tank when increasing the flow rate. At the end of the experiment, ( $T_{out}$  25 °C) with FlatICE at 4 L/min, the PCM in the bottom slabs of the tank had not completed the phase change (Figure 5) and therefore stored 8% less energy.



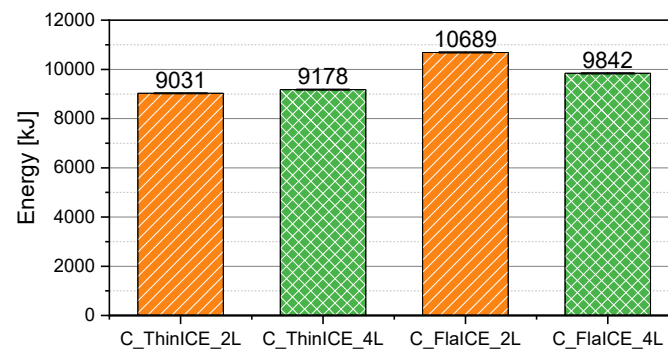


**Figure 7.** Total energy delivered to the PCM storage tank during the charging processes of the four study cases presented in this study.

### 3.3. Temperature Evolution during the Discharging Process

Figure 8 shows the discharging temperature profile of all sensors placed at the surface of the slabs at two different mass flow rates. Analyzing the influence of the PCM encapsulation design on both flow rates, the tank with ThinICE slabs finished the discharging process 30% faster than with FlatICE slabs. This can be explained by the higher heat transfer surface and the lower amount of PCM (30% less according to Table 3) when using ThinICE. Moreover, when analyzing the influence of the flow rate, Figure 8 shows that for both slab types at 4 L/min the experiments were completed 50% faster than at 2 L/min.

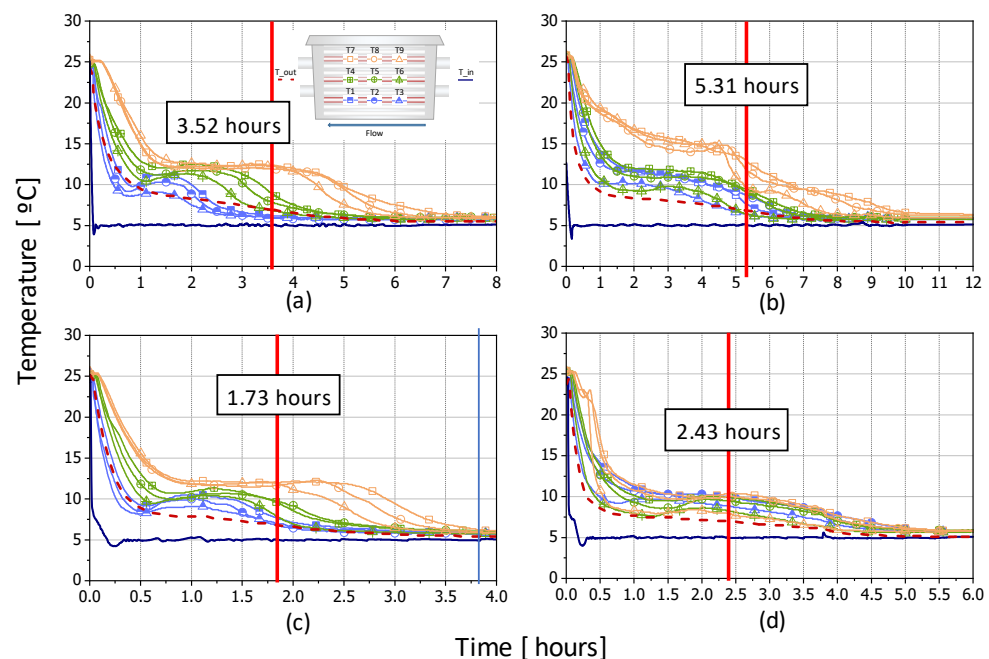


**Figure 8.** Discharge process PCM slab temperature profile for different slabs and HTF flow rates: (a) ThinICE and 2 L/min, (b) FlatICE and 2 L/min, (c) ThinICE and 4 L/min, and (d) FlatICE and 4 L/min. Note: The red line denotes the end of the charging experiment ( $T_{out} = 25^\circ\text{C}$ ). The time axis is not presented on the same scale in all the figures.

When comparing temperature distribution inside the tank (Figure 8), a similar temperature profile between the top, middle, and bottom slabs was observed in all the experiments performed with ThinICE slabs. Moreover, this behavior changed with the use of the FlatICE, where the stratification and the profile temperature inside the tank depends on the mass flow rate.

### 3.4. Heat Transfer Rate Evolution and Total Energy Released in the Discharging Process

The HTR evolution during the discharging process for all the experimental cases is shown in Figure 9. In all the experiments the profiles showed a similar trend. Significantly higher values were obtained during the first 20 min of the process when the heat is mainly transferred from the HTF inside the tank followed by an exponential decrease while the PCM decreases its temperature until minimum values are reached. Furthermore, in this case, due to the characteristics of the experimental facility, at the beginning of the experimentation the inlet temperature of the tank oscillates  $\pm 2$  °C around the desired temperature, affecting the initial peak of power. However, the inlet temperature stabilizes ( $T_{in}$  standard deviation lower than 0.3 °C) before the temperature inside the tank reaches the latent range of the PCM. After the initial peak and during the first 1.5 h of operation, ThinICE\_2L shows slightly better performance getting up to 0.1 kW more HTR than FlatICE\_2L. Moreover, due to the lower amount of PCM in the storage tank with ThinICE slabs, after 1.5 h the HTR delivered by ThinICE\_2L decreases faster than the one delivered by FlatICE\_2L. At 4 L/min, after the initial peak and during the first 1.5 h, similar results to 2 L/min are obtained. Moreover, after 1.5 h the HTR of ThinICE\_4L drastically decreases, therefore for the next 2 h (from 1.5–3.5 h) FlatICE\_4L maintains an HTR up to 0.4 kW higher than ThinICE\_2L.

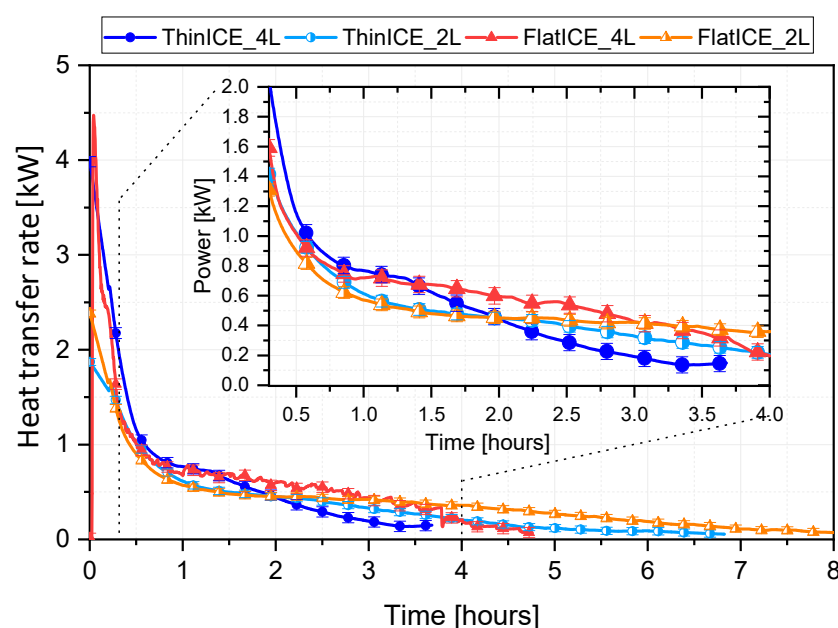


**Figure 9.** Evolution of the HTF heat transfer rate during the discharging processes of the four study cases presented in this study.

Figure 10 reports the total energy released for each experiment conditions, and the percentage it represents with respect to the energy stored in the charging process (Figure 7) in each case. Analyzing the effects of flow rate, similar to the charging, both experiments with ThinICE slabs showed a comparable energy release, suggesting a correct utilization of the energy stored in the PCM. In the case of FlatICE slabs, experiments at 2 L/min released 10% more energy compared with 4 L/min. This is supported by the fact that in the charging process the tank at 2 L/min manages to store 10% more energy than at 4 L/min (Figure 5). In addition, it is interesting to note that in all cases of the selected operating threshold approximately 85% of the energy stored in the tank was discharged.

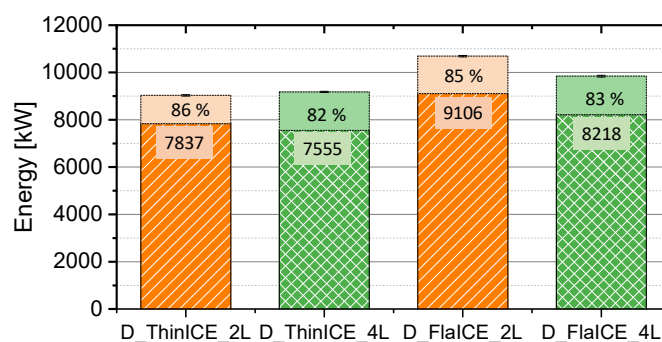


**Figure 10.** Total energy released by the PCM storage tank during the discharging processes of the four study cases presented in this study.

#### 4. Conclusions

Macro-encapsulation of phase change materials (PCM) represents one of the most widely used techniques for the implementation of latent heat thermal energy storage systems. The design of the macro-encapsulation is fundamental to archive the best compromise between optimal heat transfer performance and energy stored. However, current literature lacks experimental data on the effect of macro-encapsulation in the performance of latent heat thermal energy storage.

This paper analyzed, through an experimental study, the effect of the design of macro-encapsulated PCM on the thermal behavior of a latent heat thermal energy storage tank during both the charging and discharging processes. In this study, external dimensions of the energy storage tank were fixed and two different types of commercial slabs with different thickness filled with the same PCM were tested. The results could be particularly useful to evaluate the best configuration of storage medium when the storage tank is limited with a fixed volume.

The results were compared in terms of temperature profile, heat transfer rate, and energy stored/released. The results and the conclusions obtained from this study can be applied to similar configuration of the PCM storage that aim to use rectangular macro-encapsulated slabs as storage medium. The lesson learnt from this study suggests that macro-encapsulation design has a relevant impact on the heat transfer during both charging and discharging processes, so the design of the TES unit should be done and analyzed according to the requirements of the application.

The use of a thinner macro-encapsulation design (ThinICE) allowed fitting a larger number of slabs inside the tank. However, the higher amount of encapsulation material and the larger distance between the slabs (i.e., higher HTF channels height) resulted in a 30% less amount of PCM introduced inside the tank with this encapsulation design.

With ThinICE slabs, the temperature profiles were less affected by the influence of the mass flow rate, promoting a stratified temperature profile inside the tank in both the charging and discharging processes. Using FlatICE, this effect is more pronounced at low flow rates due to the smaller height of the channels that obstructed the flow at the bottom of the tank during charging and at the top of the tank during discharging. However, at high flow rates, the stratification is reduced with the use of thicker slabs, especially during the discharging process.

In all the discharging tests, when the outlet temperature of the tank reached 7 °C, approximately 85% of the energy previously stored in the tank was discharged.

The effect of increasing the heat transfer surface using ThinICE slabs on the power delivered by the storage tank is mostly appreciated at a higher flow rate where the heat transferred by convection is higher. Furthermore, using thinner slabs, the higher heat transfer surface area achieves a higher discharging power but is delivered for a shorter period of time. Therefore, for longer discharging periods and for higher storage capacity given a fixed volume of storage tank, the use of FlatICE should be preferred.

**Author Contributions:** Conceptualization, D.V., E.B., and L.F.C.; methodology, D.V., E.B., and G.Z.; formal analysis, D.V., E.B., A.C., B.D.M., Á.d.G., G.Z., and L.F.C.; investigation, D.V., A.C., and E.B.; resources, L.F.C.; data curation, L.F.C.; writing—original draft preparation, D.V. and E.B.; writing—review and editing, D.V., E.B., A.C., B.D.M., Á.d.G., and G.Z., L.F.C.; visualization, D.V.; supervision, L.F.C.; project administration, L.F.C.; and funding acquisition, L.F.C. All authors have read and agreed to the published version of the manuscript.

**Funding:** This project has received funding from the European Union’s Horizon 2020 research and innovation program under grant agreement No. 764025 (SWS-HEATING). This work was partially funded by the Ministerio de Ciencia, Innovación y Universidades de España (RTI2018-093849-B-C31—MCIU/AEI/FEDER, UE) and by the Ministerio de Ciencia, Innovación y Universidades—Agencia Estatal de Investigación (AEI) (RED2018-102431-T). This work is partially supported by ICREA under the ICREA Academia program.

**Institutional Review Board Statement:** Not applicable.

**Informed Consent Statement:** Not applicable.

**Data Availability Statement:** The data presented in this study are available on request from the corresponding author.

**Acknowledgments:** The authors would like to thank the Catalan Government for the quality accreditation given to their research group (2017 SGR 1537). GREiA is a certified agent TECNIO in the category of technology developers from the Government of Catalonia. Boniface Dominick Mselle would like to thank Programa Santander PredocUdL for his research fellowship. Alicia Crespo would like to acknowledge the financial support of the FI-SDUR grant from the AGAUR of the Generalitat de Catalunya and Secretaria d’Universitats i Recerca del Departament d’Empresa i Coneixement de la Generalitat de Catalunya.

**Conflicts of Interest:** The authors declare no conflict of interest.

## References

1. Borri, E.; Zsembinszki, G.; Cabeza, L.F. Recent developments of thermal energy storage applications in the built environment: A bibliometric analysis and systematic review. *Appl. Therm. Eng.* **2021**, *189*, 116666. [\[CrossRef\]](#)
2. Navarro, L.; de Gracia, A.; Colclough, S.; Browne, M.; McCormack, S.J.; Griffiths, P.; Cabeza, L.F. Thermal energy storage in building integrated thermal systems: A review. Part 1. active storage systems. *Renew. Energy* **2016**, *88*, 526–547. [\[CrossRef\]](#)
3. Navarro, L.; de Gracia, A.; Niall, D.; Castell, A.; Browne, M.; McCormack, S.J.; Griffiths, P.; Cabeza, L.F. Thermal energy storage in building integrated thermal systems: A review. Part 2. Integration as passive system. *Renew. Energy* **2016**, *85*, 1334–1356. [\[CrossRef\]](#)
4. Heier, J.; Bales, C.; Martin, V. Combining thermal energy storage with buildings—A review. *Renew. Sustain. Energy Rev.* **2015**, *42*, 1305–1325. [\[CrossRef\]](#)
5. Mselle, B.D.; Vérez, D.; Zsembinszki, G.; Borri, E.; Cabeza, L.F. Performance study of direct integration of phase change material into an innovative evaporator of a simple vapour compression system. *Appl. Sci.* **2020**, *10*, 4649. [\[CrossRef\]](#)
6. Palomba, V.; Bonanno, A.; Brunaccini, G.; Aloisio, D.; Sergi, F.; Dino, G.E.; Varvaggiannis, E.; Karellas, S.; Nitsch, B.; Strehlow, A.; et al. Hybrid cascade heat pump and thermal-electric energy storage system for residential buildings: Experimental testing and performance analysis. *Energies* **2021**, *14*, 2580. [\[CrossRef\]](#)
7. Romani, J.; Belusko, M.; Alemu, A.; Cabeza, L.F.; de Gracia, A.; Bruno, F. Control concepts of a radiant wall working as thermal energy storage for peak load shifting of a heat pump coupled to a PV array. *Renew. Energy* **2018**, *118*, 489–501. [\[CrossRef\]](#)
8. Wang, J.; Zhang, Q.; Yu, Y.; Chen, X.; Yoon, S. Application of model-based control strategy to hybrid free cooling system with latent heat thermal energy storage for TBSs. *Energy Build.* **2018**, *167*, 89–105. [\[CrossRef\]](#)
9. Yu, C.-R.; Guo, H.-S.; Wang, Q.-C.; Chang, R.-D. Revealing the impacts of passive cooling techniques on building energy performance: A residential case in Hong Kong. *Appl. Sci.* **2020**, *10*, 4188. [\[CrossRef\]](#)
10. Kameni Nematchoua, M.; Vanona, J.C.; Orosa, J.A. Energy efficiency and thermal performance of office buildings integrated with passive strategies in coastal regions of humid and hot tropical climates in Madagascar. *Appl. Sci.* **2020**, *10*, 2438. [\[CrossRef\]](#)
11. Prieto, C.; Fereres, S.; Cabeza, L.F. The role of innovation in industry product deployment: Developing thermal energy storage for concentrated solar power. *Energies* **2020**, *13*, 2943. [\[CrossRef\]](#)
12. Palomba, V.; Brancato, V.; Frazzica, A. Experimental investigation of a latent heat storage for solar cooling applications. *Appl. Energy* **2017**, *199*, 347–358. [\[CrossRef\]](#)
13. Guelpa, E.; Verda, V. Thermal energy storage in district heating and cooling systems: A review. *Appl. Energy* **2019**, *252*, 113474. [\[CrossRef\]](#)
14. Miró, L.; Gasia, J.; Cabeza, L.F. Thermal energy storage (TES) for industrial waste heat (IWH) recovery: A review. *Appl. Energy* **2016**, *179*, 284–301. [\[CrossRef\]](#)

15. Crespo, A.; Barreneche, C.; Ibarra, M.; Platzer, W. Latent thermal energy storage for solar process heat applications at medium-high temperatures—A review. *Sol. Energy* **2019**, *192*, 3–34. [CrossRef]
16. Borri, E.; Sze, J.Y.; Tafone, A.; Romagnoli, A.; Li, Y.; Comodi, G. Experimental and numerical characterization of sub-zero phase change materials for cold thermal energy storage. *Appl. Energy* **2020**, *275*, 115131. [CrossRef]
17. Mehling, H.; Cabeza, L.F. *Heat and Cold Storage with PCM. An Up to Date Introduction into Basics and Applications*, 1st ed.; Springer: Berlin/Heidelberg, Germany, 2008; ISBN 979-3-540-68556-2.
18. Gasia, J.; Tay, N.H.S.; Belusko, M.; Cabeza, L.F.; Bruno, F. Experimental investigation of the effect of dynamic melting in a cylindrical shell-and-tube heat exchanger using water as PCM. *Appl. Energy* **2017**, *185*, 136–145. [CrossRef]
19. Huang, K.; Liang, D.; Feng, G.; Jiang, M.; Zhu, Y.; Liu, X.; Jiang, B. Macro-encapsulated PCM cylinder module based on paraffin and float stones. *Materials* **2016**, *9*, 361. [CrossRef]
20. Besagni, G.; Croci, L. Experimental study of a pilot-scale fin-and-tube phase change material storage. *Appl. Therm. Eng.* **2019**, *160*, 114089. [CrossRef]
21. Liu, Z.; Yu, Z.J.; Yang, T.; Qin, D.; Li, S.; Zhang, G.; Haghighat, F.; Joybari, M.M. A review on macro-encapsulated phase change material for building envelope applications. *Build. Environ.* **2018**, *144*, 281–294. [CrossRef]
22. Khudhair, A.M.; Farid, M.M. A review on energy conservation in building applications with thermal storage by latent heat using phase change materials. *Energy Convers. Manag.* **2004**, *45*, 263–275. [CrossRef]
23. Chandel, S.S.; Agarwal, T. Review of current state of research on energy storage, toxicity, health hazards and commercialization of phase changing materials. *Renew. Sustain. Energy Rev.* **2017**, *67*, 581–596. [CrossRef]
24. Sun, X.; Chu, Y.; Medina, M.A.; Mo, Y.; Fan, S.; Liao, S. Experimental investigations on the thermal behavior of phase change material (PCM) in ventilated slabs. *Appl. Therm. Eng.* **2019**, *148*, 1359–1369. [CrossRef]
25. Carmona, M.; Rincón, A.; Gulfo, L. Energy and exergy model with parametric study of a hot water storage tank with PCM for domestic applications and experimental validation for multiple operational scenarios. *Energy Convers. Manag.* **2020**, *222*, 113189. [CrossRef]
26. Xu, T.; Humire, E.N.; Chiu, J.N.-W.; Sawalha, S. Numerical thermal performance investigation of a latent heat storage prototype toward effective use in residential heating systems. *Appl. Energy* **2020**, *278*, 115631. [CrossRef]
27. Goeke, J.; Schwaborn, E. Phase change material in spherical capsules for hybrid thermal storage. *Chem. Ing. Tech.* **2020**, *92*, 1098–1108. [CrossRef]
28. Erlbeck, L.; Schreiner, P.; Schlachter, K.; Dörnhöfer, P.; Fasel, F.; Methner, F.J.; Rädle, M.A. of thermal behavior by changing the shape of P. inclusions in concrete blocks Adjustment of thermal behavior by changing the shape of PCM inclusions in concrete blocks. *Energy Convers. Manag.* **2018**, *158*, 256–265. [CrossRef]
29. Al-Yasiri, Q.; Szabó, M. Thermal performance of concrete bricks based phase change material encapsulated by various aluminium containers: An experimental study under Iraqi hot climate conditions. *J. Energy Storage* **2021**, *40*, 102710. [CrossRef]
30. Ismail, K.A.R.; Moraes, R.I.R. A numerical and experimental investigation of different containers and PCM options for cold storage modular units for domestic applications. *Int. J. Heat Mass Transf.* **2009**, *52*, 4195–4202. [CrossRef]
31. Moreno, P.; Castell, A.; Solé, C.; Zsembinszki, G.; Cabeza, L.F. PCM thermal energy storage tanks in heat pump system for space cooling. *Energy Build.* **2014**, *82*, 399–405. [CrossRef]
32. D'Avignon, K.; Kummert, M. Experimental assessment of a phase change material storage tank. *Appl. Therm. Eng.* **2016**, *99*, 880–891. [CrossRef]
33. Liu, M.; Saman, W.; Bruno, F. Validation of a mathematical model for encapsulated phase change material flat slabs for cooling applications. *Appl. Therm. Eng.* **2011**, *31*, 2340–2347. [CrossRef]
34. Hosseini, M.J.; Ranjbar, A.A.; Sedighi, K.; Rahimi, M. A combined experimental and computational study on the melting behavior of a medium temperature phase change storage material inside shell and tube heat exchanger. *Int. Commun. Heat Mass Transf.* **2012**, *39*, 1416–1424. [CrossRef]
35. PCM Products. Available online: <http://www.pcmproducts.net/> (accessed on 15 January 2019).
36. Zanotti. Available online: <https://zanottiappliance.com/es/refrigeracion/refrigeracion-fija/> (accessed on 18 June 2021).
37. OVAN. Available online: <https://ovan.es/> (accessed on 18 June 2021).
38. SELECTA. Available online: <https://grupo-selecta.com/distribuidores/esli-sarl-engineering-scientific-lab-instruments/> (accessed on 18 June 2021).
39. Badgermeter. Available online: <https://www.badgermeter.com/es-es/productos/medidores/medidores-de-flujo-electromagneticos/medidor-de-flujo-electromagnetico-modmag-m1000/> (accessed on 18 June 2021).
40. Step DI-01. Available online: <https://store.stepsl.com/product?prod=DL-01> (accessed on 18 June 2021).
41. Indusoft Web Studio. Available online: <https://www.aveva.com/en/products/indusoft-web-studio/> (accessed on 18 June 2021).
42. Kukulka, D. *Thermodynamic and Transport Properties of Pure and Saline Water*; State University of New York: Buffalo, NY, USA, 1981.
43. Holman, J. *Experimental Methods for Engineers*, 8th ed.; McGraw-Hill: New York, NY, USA, 2012; ISBN 0073529303.